ELSEVIER

Contents lists available at ScienceDirect

# **Optics Communications**

journal homepage: www.elsevier.com/locate/optcom





# Modulated high-order Hermite-Gaussian beams with uniform intensity distribution

Emma M. Sundin <sup>a</sup>, Gilberto Navarro <sup>b</sup>, Chunqiang Li <sup>b,\*</sup>

- a Department of Metallurgical, Materials, and Biomedical Engineering, The University of Texas at El Paso, 500 W University Avenue, El Paso, TX, 79968, USA
- b Department of Physics, The University of Texas at El Paso, 500 W University Avenue, El Paso, TX, 79968, USA

#### ARTICLE INFO

Key Terms: Hermite-Gaussian beams Spatial phase modulation

## ABSTRACT

Hermite-Gaussian beams have been studied since the early years of laser modes. With the recent development of structured light, different modulation methods have been demonstrated to control the energy, polarization and propagation behavior of Hermite-Gaussian beams. In this work we introduce an inverse design approach to modulate the energy distribution among different lobes of Hermite-Gaussian beams. In this approach, the desired intensity profiles of Hermite-Gaussian beams are the starting point. The required spatial phase masks are calculated through inverse Fourier transform, then projected on a spatial light modulator to convert conventional Gaussian beams into modulated Hermite-Gaussian beams. The experimental modulated high-order (m = 10, n = 10) Hermite-Gaussian beams show much improved energy distribution among different lobes over standard Hermite-Gaussian beams. These modulated Hermite-Gaussian beams also have improved beam quality factor  $M^2$  after modulation. These results demonstrated the feasibility to fine-tune the intensity profiles of Hermite-Gaussian beams, which have applications in structured illumination, particle manipulation and optical communications.

## 1. Introduction

In recent years structured light has attracted great interests in both fundamental physics such as orbital angular momentum of light, and broad applications in optical/quantum communications, optical tweezers, and laser-based manufacturing [1]. Hermite-Gaussian (HG) beams have been discovered in the early years of laser research [2]. When the argument in Hermite-Gaussian functions is complex [3], the resulting laser beams are named as elegant HG beams with structural instability, i. e., the transverse beam intensity changes during propagation [4,5]. Mathematically, HG modes can be expressed as the sum of Laguerre-Gaussian (LG) modes, and vice versa [6]. Therefore, it is not surprising that HG beams can also acquire orbital angular momentum via linear combination of two or more HG beams with certain phase shifts [7,8]. Generalized HG modes constructed from summation of normal HG modes can describe both HG and LG modes by varying a characteristic function [9]. This unified theory provides a useful approach to analyze mode transformations. One advantage of structured light is its potential to overcome medium scattering and turbulence. Although current results are still contradictory [10], it has been demonstrated that a subset of HG beams is more resilient to atmospheric

turbulence while using different HG modes to transmit information [11]. A theoretical and experimental investigation shows that after a HG mode is partially blocked, it can recover its original mode or transfer to a lower order mode due to incoherent or coherent interference of multiple eigenmodes [12]. In some applications such as optical trapping [13,14], structured illumination microscopy [15,16], and optical lithography [17], it is desirable to use square or hexagonal lattice beams with uniform intensities among all beam lobes. Although HG beams have a square lattice shape, the intensities in middle lobes are much lower than those of side lobes. Inverse design of the phase modulation for generating arbitrary 3D nanostructures has been demonstrated [18]. Such an approach does not have the non-diffracting property of many structured light beams making it difficult to achieve large 3D structures. One appealing approach is to use quasi-non-diffracting beams with phase modulation to obtain designed structures [19]. Such beams are not actually non-diffracting but can still maintain their intensity profile over large distances. Modulated HG beams have been demonstrated with more evenly distributed energy among lobes [20,21]. This method introduces a  $\pi$ -phase shift in the annular phase mask, thus modulating the energy distribution. These results are demonstrated with low order HG<sub>m</sub>.  $_{n}$  beams only (m = 3, n = 3). In principle it is difficult to control a large

<sup>\*</sup> Corresponding author.

E-mail address: cli@utep.edu (C. Li).

number (e.g. hundreds) of beam intensities in higher order HG beams with such a single-phase shift. In this work we developed an inverse design approach to enhance the intensities of middle lobes to achieve uniform intensity distribution among lobes in higher order HG beams (m = 10, n = 10, and m = 20, n = 20 as two examples). In principle higher order modes can carry more information as their values in each degree of freedom have an expanded range over lower order modes. Theoretical analysis shows that the beam quality  $M^2$  factor of higher order modes is less affected by air turbulence than lower order modes, indicating their advantages in long-distance free-space optical communications [22].

#### 2. Methods

In this inverse design approach, the standard Hermite-Gaussian equations are used to calculate the beam intensities and phases of standard HG beams (Box I in Fig. 1). The fast Fourier Transform (FFT) result of the phase profile gives the electric field of a standard HG beam. A pre-determined 2D envelope function times this standard HG beam will result in a modulated HG beam with uniform intensities (Box II in Fig. 1). Inverse FFT (IFFT) on this modified electric field distribution gives the profile of the phase mask (Box III in Fig. 1). The real part (*Re(J*)) of this complex result is displayed on a spatial light modulator (SLM) to convert a conventional Gaussian beam into a modulated HG beam (Box IV in Fig. 1).

In terms of mathematics the modulated HG beam (mHG) is the product of a standard HG beam (sHG) and the envelop function (Env) in real space (Eq. (1)). This Env function is a slowly varying function compared with the sHG function.

$$mHG(x, y) = sHG(x, y) \times Env(x, y)$$
 (1)

After Fourier transform in k-space the modulated HG beam is a convolution of the standard HG beam phase and the transformed envelope function (Eq. (2)).

$$mHG(k_x, k_y) = sHG(k_x, k_y) * Env(k_x, k_y) = \int_{-\infty}^{+\infty} sHG(k_x - u, k_y - v)$$

$$\times Env(u, v) \ dudv$$
(2)

The standard HG beam in k-space is the phase mask we used for beam generation in Box I. Because this envelope function is a slowly varying function, in k-space it has low frequency components only. Thus, the integral range is  $(-\varepsilon, +\varepsilon)$ , where  $\varepsilon$  is much smaller than  $k_x$  and  $k_y$ . For any k-vector in the modulated beam, the convolution integral will have contributions only from a small region around this k-vector of the

standard beam. The overall effect is to slightly modify the standard HG beam phase mask i.e. qualitatively smoothing out the sharp edges and reducing the phase contrast as shown in the modified phase mask in Box III.

The optical setup is illustrated in Fig. 2(a). A femtosecond Ti/sapphire laser (Spectra-Physics Mai Tai HP) outputs Gaussian beams at 710 nm. The beam is expanded through a telescope to match the size of the liquid crystal on silicon (LCOS) display based spatial light modulator (SLM, HES 6001 microdisplay with 0.7" diagonal,  $1920 \times 1080$  with 8.0 μm pixel pitch, HOLOEYE Photonics). Diffraction efficiency when using binary gratings with this SLM was found to be dependent on the polarization angle of the incident light. To maximize power in the first order beams, a polarizing beam splitter (PBS) cube and half-wave plate were added to the optical path before the SLM to rotate the linear polarization of the illumination to an optimal angle. Fig. 2(b) & (c) show two phase masks displayed on the SLM for standard and modulated HG<sub>10.10</sub> beams respectively. Compared with the standard HG mask, the modulated HG mask shows soft edges in its phase pattern. Since the modulated HG beam is achieved by applying an envelope function on the standard HG beam in real space, in phase space the modulated HG beam mask is the convolution of the standard HG beam mask and the Fourier transform of the envelop function which is a slowly varying function. Hence, this convolution operation will lead to soft edges in the modulated HG phase mask. This Gaussian beam is converted into a HG beam after SLM, and is further focused by a lens (f = 500 mm) to form an image on a CMOS camera (1280  $\times$  1024 with 3.6  $\mu m$  pixel pitch, DCC1645C, Thorlabs). A linear polarizer is placed after the focusing lens to remove background noise. The camera is mounted on a translational stage to move in the beam propagation direction (z) to acquire images at different propagation distances. While acquiring images at different zlocations for one HG beam, the camera exposure time and gain are kept at the same values in order to compare beam intensity variation along the z-direction. A standard HG phase mask, when applied to a phase modulation SLM, will directly convert an incident Gaussian beam into a standard HG beam. However, because the experimental beams presented in this work were produced using a reflective microdisplay, diffraction gratings were needed to diffract the desired HG beams in the higher orders while leaving the residual Gaussian beam in the zeroth order. Therefore, binary diffraction gratings were added to both the standard and modulated phase masks, and the resulting HG beams are diffracted into the first-order in the horizontal direction. For our experimental setup, an 18-pixel (144 µm) period vertical grating was found to provide enough angular separation between the zeroth-order and first-order beams to minimize interference from zeroth-order. When the grating period is smaller, we found that the intensity

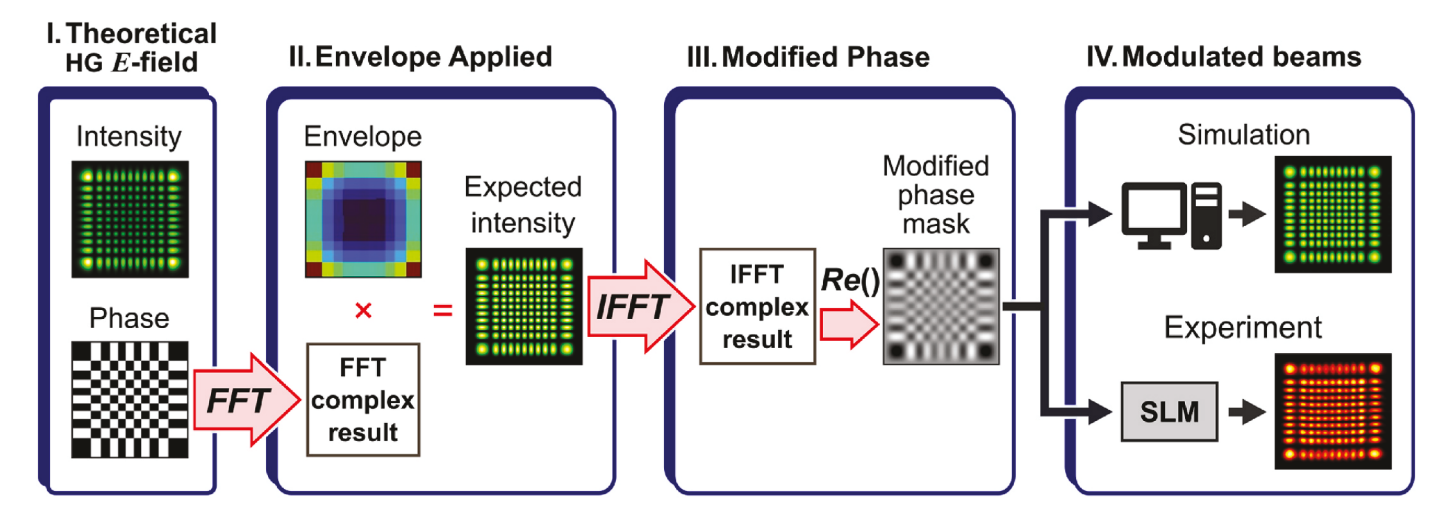
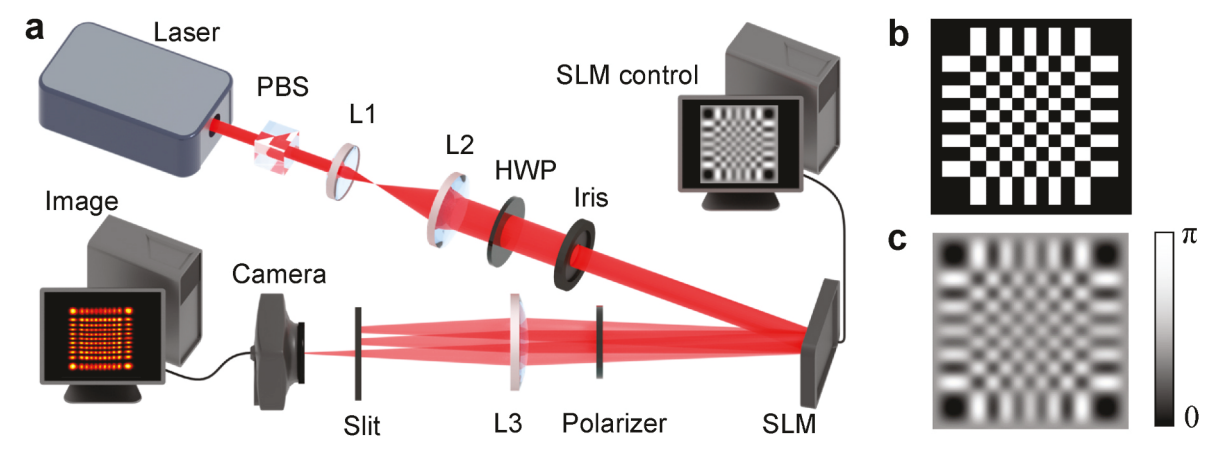


Fig. 1. Flow chart of the inverse design of modulated HG beams with uniform intensity.



**Fig. 2.** (a) Optical setup of the HG beam generation and propagation measurement. PBS: polarizing beam splitter, HWP: half-wave plate, SLM: spatial light modulator. (b) Phase mask for standard  $HG_{10,10}$  beam. (c) Phase mask for modulated  $HG_{10,10}$  beam.

between adjacent lobes in the horizontal direction did not go down to zero as expected while such phenomenon did not happen in the vertical direction. The possible reason is that the grating phase pattern is combined with the HG beam phase. The overall phase has a much larger modulation depth than either of the two phases. This may cause experimental errors in both the grating and HG phases, thus reducing the diffraction efficiency and the quality of the HG beam.

The propagation of HG beams is also numerically simulated with LightPipes software package to compare with experimental results [23]. The specific beam propagation calculation method is "Fresnel", which calculates direct integration as a convolution. The simulations were set up as follows: a square aperture the size of the phase mask (1080  $\times$  1080 pixels) was applied to a constant-intensity field (2160  $\times$  2160 pixels) to obtain a flat-top square beam as the starting beam; to this starting beam, a standard or modified HG phase mask was applied, and the beam propagated to a lens of focal-length matching that used in the experimental setup; around the focal point of the lens, transverse profiles of simulated beam intensity were obtained to compare with experimental results. Simulation variables, e.g., illumination wavelength, phase mask physical dimensions, lens distance, and focal length, were matched to those in the experimental setup described above. When an 18-pixel (144 um) period grating was added to HG phase masks, the simulated HG beams showed noticeably greater distortion from the zeroth-order Gaussian beam compared to the experimental HG beams. This may possibly be due to the starting beam being a flat-top square beam, which has an abrupt edge that causes stronger diffraction. To bring simulated beam distortion closer in line with experimental results, a finer grating (2-pixel period, 16 µm) was used for the simulated beams. Apart from reducing the extra distortion from the zeroth-order, use of this finer grating did not change the appearance of the simulated beams.

To quantify the beams' properties for comparison, image data collected from the simulations and experiments were analyzed to calculate the linear width, second-order moment width, and intensity distribution. Because the vertical diffraction gratings that were applied to the phase masks introduced a slight horizontal distortion to the beams, all widths were calculated along the vertical direction (y), which was unaffected by this distortion. Linear beam width defined as the HG beam square side length was measured as the mean vertical distance between the centroids of the beams' corner lobes. Second-order moment width  $(2\sigma)$  was defined as the square root of the second-order moment of the transverse intensity profile of the standard and modulated HG beams. While calculating  $2\sigma$  width, it is important to reduce the contribution from the noisy background and asymmetry of the beam intensity distribution. For both simulation and experimental images, the beams were cropped to size to eliminate most of the background and any features not part of the main beam. For the experimental images, the noise floor was removed during the width calculations by subtracting

the minimum of the horizontal intensity sum from that profile (i.e., the x-independent integral in dx) before proceeding with the y-dependent integral. No noise-floor subtraction was needed for the simulations. To further characterize the beams, values for the beam quality factor, beam waist width, and waist position were determined by fitting the  $2\sigma$  widths calculated as described above to the function [24,25] w(z)=

 $\sqrt{w_0 + M^4 \left(\frac{\lambda}{\pi w_0}\right)^2 (z-z_0)^2}$ , where w is  $2\sigma$  width, z is propagation distance measured from a fixed point,  $\lambda$  is the beam's wavelength,  $M^2$  is the beam quality factor,  $w_0$  is the  $2\sigma$  width at the waist, and  $z_0$  is the z-location of the beam waist. The three variables w, z, and  $\lambda$  were known from experimental measurements, while  $M^2$ ,  $w_0$ , and  $z_0$  were fitting parameters. Best-fit values of  $M^2$ ,  $w_0$ , and  $z_0$  for all simulated and experimental beams shown in this paper are presented in Table 1.

## 3. Results

The simulated standard HG beams are shown in Fig. 3(a) & 3(b) at different propagation distances with  $\Delta z = \pm 50$  mm. The images in Fig. 3 (a) demonstrate that the HG beam intensity changes on both sides of the focus, which coincides with the theoretical expectation. In order to compare intensities in different parts of the beam, profiles were taken in each image along two vertical lines, one along the edge lobes and the other along the center lobes, to plot their intensities (Fig. 3(b)). In all these plots the intensity is normalized to the highest pixel value in each series of images for comparison. These plots confirm the characteristics of standard HG beams. The simulated modulated HG beams are shown in Fig. 3(c) and (d) in the same propagation range. For these modulated beams, overall beam shape is identical to the standard HG beams, while intensity distribution is much more even among the different lobes. For instance, in the  $\Delta z = 0$  mm plane image, the intensities of the center lobes are about 80-90 % of the intensities of the brightest corner lobes. As the beam propagates away from the focus, the unevenness of lobe intensities becomes larger. These simulation results show the promise of improving the uniformity of beam lobe intensities. The experimental results of standard and modulated HG beams are shown in Fig. 3(e) - 3 (h). The images of the standard HG beam in Fig. 3(e) follow the simulated results in Fig. 3(a). The experimental modulated HG beam (Fig. 3 (g)) also shows strong similarity to simulation (Fig. 3(c)). At  $\Delta z = 0$  mm plane, quantitative analysis shows that the center lobes are about 60-70 % of the brightest corner lobes (Fig. 3(h)), which is lower than the values in simulation (Fig. 3(d)). However, the center column intensities are as high as the side column intensities except the corners, which is a significant improvement over standard HG beam (Fig. 3(f)). As the modulated HG beam propagates to and from focus, the intensities of corner lobes increase, while the center lobes' intensities decrease. The

**Table 1**Fitting results for standard and modulated HG beams<sup>a</sup>.

Beam	$M^2$			$w_0$ (mm)		$z_0$ (mm)	
	Theoretical	Simulation	Experiment	Simulation	Experiment	Simulation	Experiment
HG <sub>10,10</sub>							
Standard	21	21.54	21.18	0.52	0.53	2.28	-1.01
Modulated	_	21.00	20.74	0.43	0.43	1.38	-1.82
$HG_{20,20}$							
Standard	41	40.96	40.88	0.99	1.01	7.14	0.91
Modulated	-	39.85	40.79	0.74	0.78	2.71	-2.53

aFor all fitting results,  $r^2 > 0.995$ .

observed phenomenon agrees with simulation results. Theoretically the HG beams possess  $C_4$  rotational symmetry around z-axis. However, the experimental phase mask has a binary grating added to the HG phase mask with the grating wavevector in the x-direction. Hence, the experimental HG beams do not have x- and y-direction symmetry. This property is manifested in the intensity profiles in the x- and y-directions. In between two peaks the beam intensity drops to zero as shown in Fig. 3 (f) and (g) along the y-direction. Along the x-direction, on the contrary, this intensity does not go down to zero. This experimental noise comes from the diffraction grating, which gives slight noise in the  $\pm 1$  diffracted orders as discussed in the Methods section. Implementing other types of spatial light modulators without a diffraction grating, such as phase only SLM, will remove this experimental noise.

To further visualize the beams' propagation behavior, beam intensities in the center ( $\Delta x = 0$ ) longitudinal plane (y-z) are shown in Fig. 4 (a)-(d). The standard Hermite-Gaussian beams show high intensity in the edge lobes and much lower intensity in the inner lobes. In comparison, the modulated beams show much more even intensity among the center and edge lobes. This increased brightness in the inner lobes of the beam extends from about -25 mm to +25 mm in  $\Delta z$  measured from the focus. Beyond of this  $\Delta z$  range inner lobe intensity quickly decreases with increasing distance from the focus. It can be observed that the experimental beams do not have symmetrical intensity behavior in z. This can be explained by experimental errors. Fig. 4 (e) shows the quantitative intensity variations while both the standard and modulated HG beams propagate along the z-direction. The intensity of corner lobes of this standard HG<sub>10.10</sub> beam has a peak at  $\Delta z = 0$  mm with full width at half maximum (FWHM) about 50 mm. The intensity of center lobes of this standard HG<sub>10,10</sub> beam is only about 10-20 % of its corner lobe intensity. The intensity of corner lobes of this modulated HG<sub>10,10</sub> beam shows small variations (<25 %) in the range of  $\Delta z=\pm50$  mm. The intensity of center lobes of this modulated  $HG_{10,10}$  beam is about 60–70 % of its corner lobe intensity in the range of  $\Delta z = \pm 20$  mm, and the FWHM

The divergence of a beam over propagation is an important property which determines energy concentration and radiation pressure. The straightforward way of quantifying HG beam divergence is to measure the square beam size. Fig. 5(a) shows the square shape width of standard and modulated HG beams over propagation. The width of the modulated HG beam is the same as the standard HG beam over a distance of 150 mm indicating the modulated HG beam also has quasi non-diffracting property. Within the  $\Delta z = \pm 20$  mm distance the beam width has no significant change, which has the potential to form 3D uniform light fields. The more rigorous way of characterizing a laser beam's propagation is to calculate the second-order moment of its intensity distribution, i.e., the beam quality factor  $M^2$ . The beam widths  $(2\sigma)$  defined as the square roots of the second-order moments of experimental standard and modulated HG beams are shown as scattered points together with the second-order moments of simulated standard and modulated HG beams shown as dashed lines in Fig. 5(b). This plot shows a close resemblance between simulated beam widths and experimental beam widths. The  $2\sigma$  beam widths of modulated beams are expected to be

smaller than those of standard beams, as the intensities are distributed more evenly among lobes, which results in smaller second-order moments. This is true only within  $\Delta z=\pm 50$  mm range. While  $|\Delta z|>50$  mm, the beam widths of modulated beams are larger than those of standard beams. This shows that the modulated beam diverges faster while propagating away from the focal point. The  $M^2$  factors in Table 1 are calculated by fitting the above equation to the data sets in Fig. 5(b). Theoretically the propagation factor  $M^2$  of a standard  $\mathrm{HG}_{\mathrm{m,n}}$  beam in one lateral dimension equals 2 m + 1 or 2n+1 [26,27], which is 21 for  $\mathrm{HG}_{10}$ ,  $_{10}$  beams. The simulated and experimental standard  $\mathrm{HG}_{10,10}$  beams'  $M^2$  factors are 21.54 and 21.18 respectively, which are slightly larger than 21 as shown in Table 1. This demonstrates that these experimental beams are close to theoretical beams. The  $M^2$  factors of simulated and experimental modulated beams are 21.00 and 20.74 respectively. These values show improved beam quality factor.

Furthermore, the same modulation method was applied to the  $\mathrm{HG}_{20,20}$  beams to test its feasibility on even higher order modes. The overall performance on this higher order mode is similar to the results of  $\mathrm{HG}_{10,10}$  beam (Fig. 6). At  $\Delta z=0$  mm plane, the intensities of the center lobes are about 50–60 % of the intensities of the brightest corner lobes. The intensities among different lobes are less uniform than in the lower order beams (Fig. 7 vs. Fig. 4). The beam width of the modulated  $\mathrm{HG}_{20,20}$  beam also followed the same trend as the  $\mathrm{HG}_{10,10}$  beam (Fig. 8). One difference is that the  $2\sigma$  beam widths of modulated  $\mathrm{HG}_{20,20}$  beams were smaller than those of standard beams over an extended range  $\Delta z=\pm75$  mm (Fig. 8(b)).

#### 4. Discussion

We have developed an inverse design approach to modulate lobe intensities in Hermite-Gaussian beams. By theoretically calculating the spatial phase for a predetermined HG beam intensity pattern, this method achieved uniform distribution among lobe intensities for highorder modes (m = 10, n = 10 and m = 20, n = 20). These modulated HG beams propagate over an extended range  $\Delta z = \pm 20$  mm while maintaining their intensity profiles. Their beam quality factors are better than their counterpart standard HG beams. In the current setup an amplitude modulation display is used to convert Gaussian beams into HG beams, which requires adding a diffraction grating to the phase mask. For standard Hermite-Gaussian beams, the intensity of first order beams is comparable to the zeroth-order beam. However, the diffraction efficiency dropped significantly, and the modulated HG beam intensity is only about 25 % of the standard HG beams. This is probably due to the reduced phase modulation amplitude in the modulated HG phase mask as shown in Fig. 2. Using a phase modulation SLM can greatly improve the conversion efficiency. The intensity fluctuations among different lobes are still significant for these modulated HG beams. There are two possible reasons for this phenomenon. While modulated HG beams propagate, the intensity of each lobe fluctuates along this path as demonstrated by both experimental results and simulations. Another reason comes from experimental errors. Further investigation on this direction will lead to more uniform distribution of beam intensities.

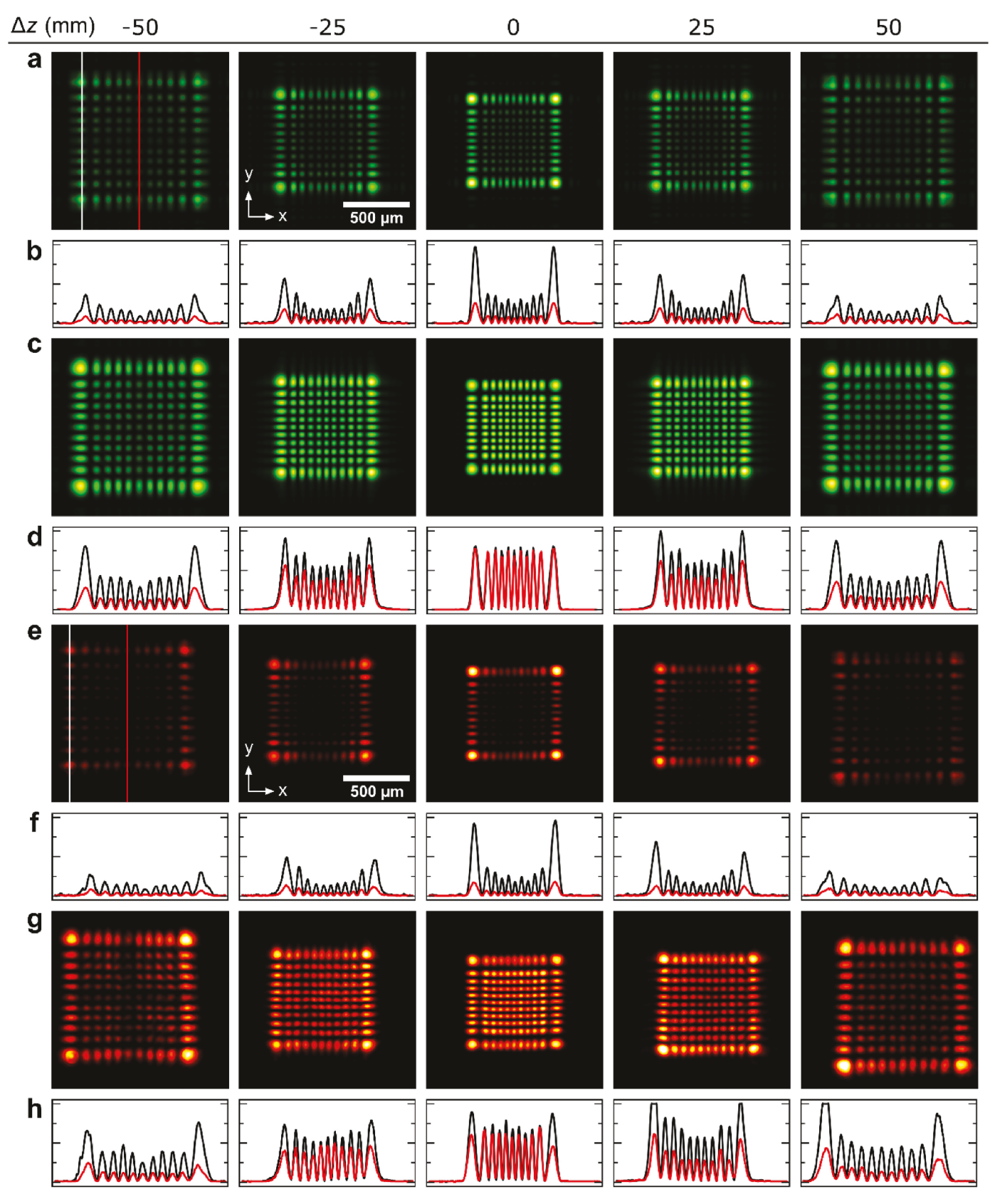
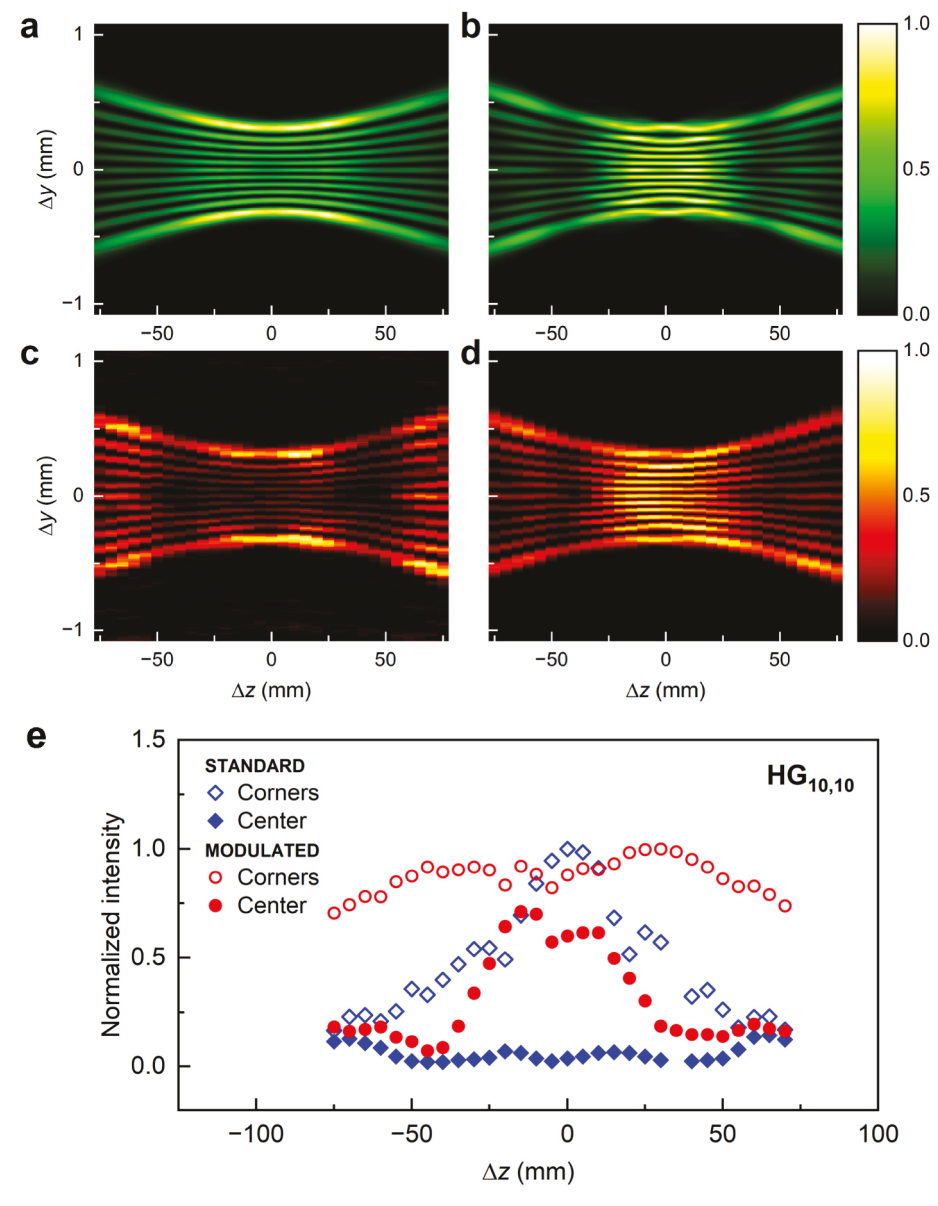


Fig. 3. Standard and modulated HG<sub>10,10</sub> beams. (a) Simulated standard HG beam intensity images at different z locations. (b) Intensity plots of standard HG beams along the two vertical lines drawn in (a). (c) Simulated modulated HG beam intensity images at different z locations. (d) Intensity plots of modulated HG beams along the two vertical lines drawn in (a). (e) Experimental standard HG beam intensity images at different z locations. (f) Intensity plots of standard HG beams along the two vertical lines drawn in (e). (g) Experimental modulated HG beam intensity images at different z locations. (h) Intensity plots of modulated HG beams along the two vertical lines drawn in (e).



**Fig. 4.** Standard and modulated  $HG_{10,10}$  beams in *y-z* plane. (a) Simulated standard HG beam. (b) Simulated modulated HG beam. (c) Experimental standard HG beam. (d) Experimental modulated HG beam. (e) Intensity, normalized to global maximum for each *z*-scan, of corner and center beam-lobes.

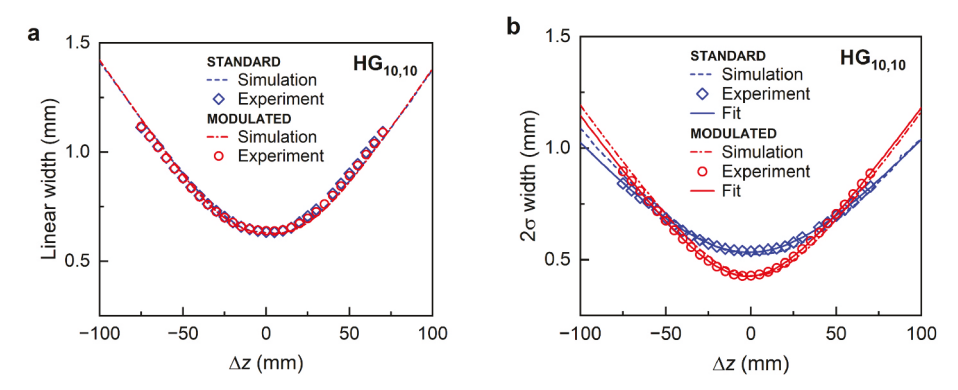


Fig. 5. Beam width of simulated and experimental  $HG_{10,10}$  measured as a) linear width (edge-to-edge height of beam measured as vertical distance between centroids of corner lobes), and b) second-order moment width ( $2\sigma$ ).

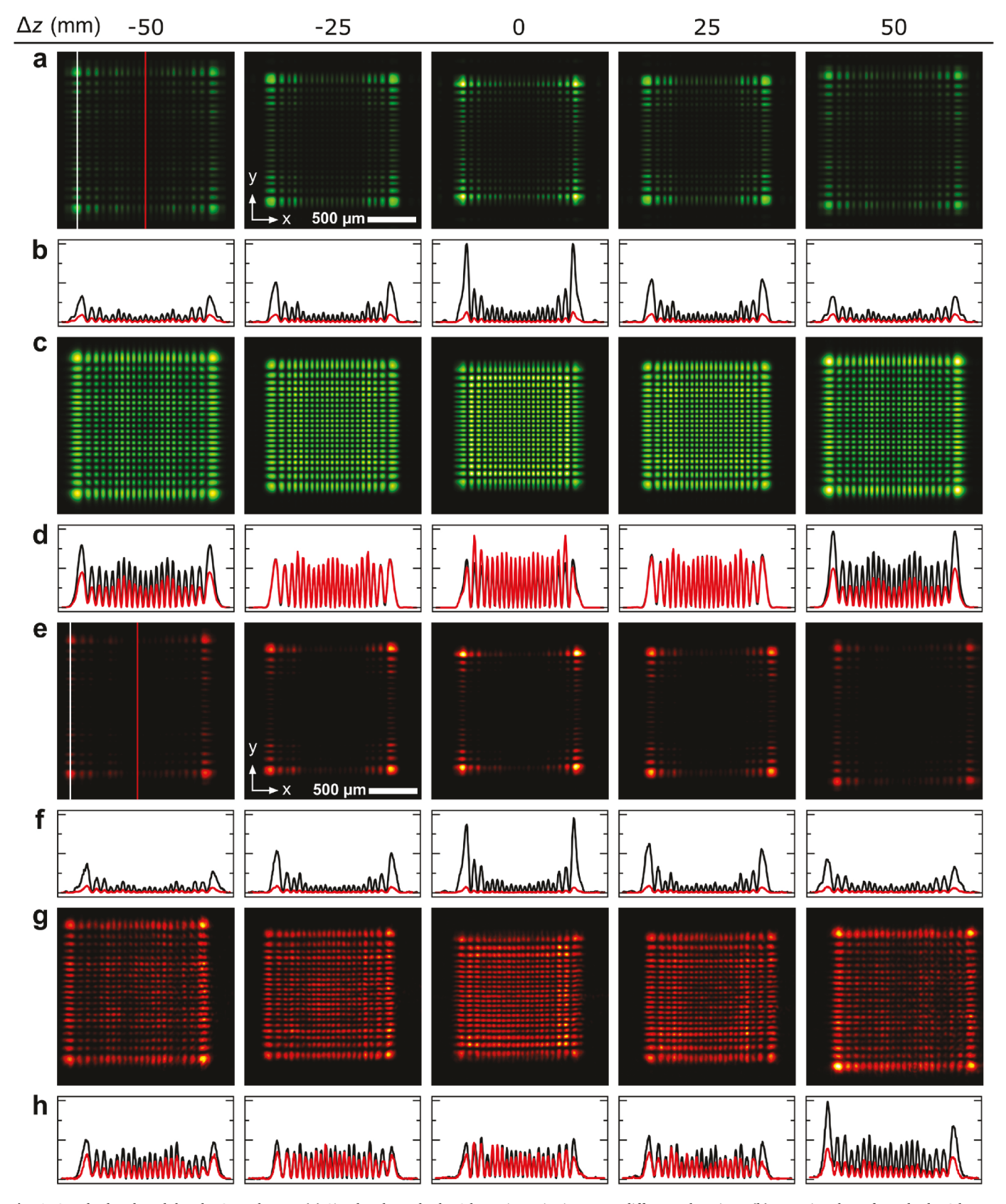


Fig. 6. Standard and modulated  $HG_{20,20}$  beams. (a) Simulated standard HG beam intensity images at different z locations. (b) Intensity plots of standard HG beams along the two vertical lines drawn in (a). (c) Simulated modulated HG beam intensity images at different z locations. (d) Intensity plots of modulated HG beams along the two vertical lines drawn in (a). (e) Experimental standard HG beam intensity images at different z locations. (f) Intensity plots of standard HG beams along the two vertical lines drawn in (e). (g) Experimental modulated HG beam intensity images at different z locations. (h) Intensity plots of modulated HG beams along the two vertical lines drawn in (e).

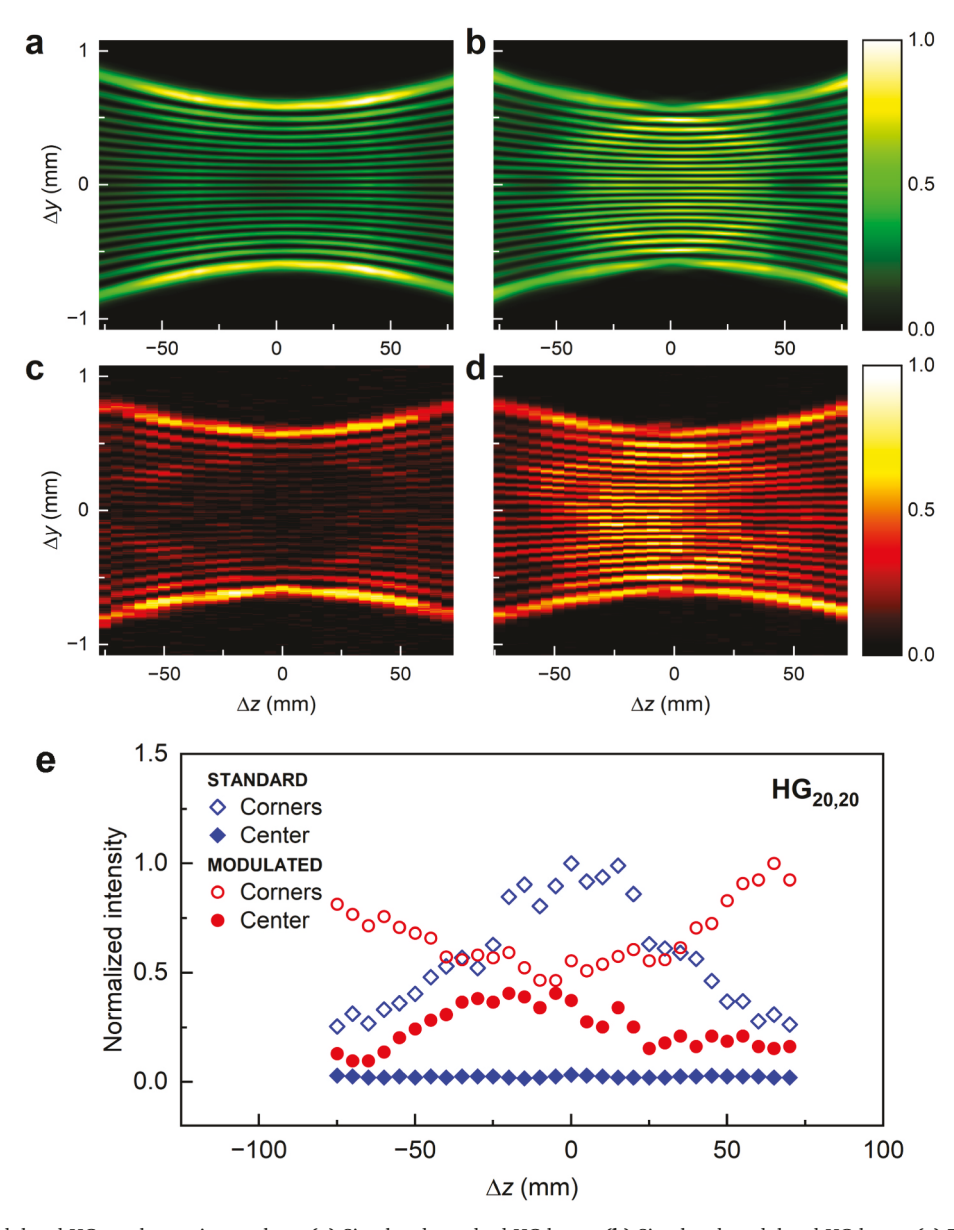


Fig. 7. Standard and modulated  $HG_{10,10}$  beams in y-z plane. (a) Simulated standard HG beam. (b) Simulated modulated HG beam. (c) Experimental standard HG beam. (d) Experimental modulated HG beam. (e) Intensity, normalized to global maximum for each z-scan, of corner and center beam-lobes.

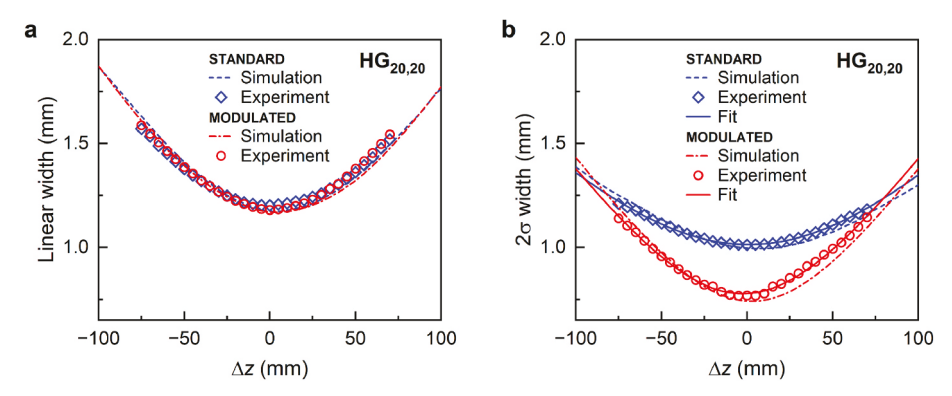


Fig. 8. Beam width of simulated and experimental  $HG_{20,20}$  measured as a) linear width (edge-to-edge height of beam measured as vertical distance between centroids of corner lobes), and b) second-order moment width ( $2\sigma$ ).

These modulated HG beams form uniform intensity lobes in two dimensions only. By interfering several modulated HG beams uniform intensity, 3D lattices can be formed for many applications in future.

#### CRediT authorship contribution statement

**Emma M. Sundin:** Data curation, Formal analysis, Methodology, Visualization, Writing – review & editing. **Gilberto Navarro:** Data curation, Methodology. **Chunqiang Li:** Conceptualization, Data curation, Formal analysis, Funding acquisition, Investigation, Methodology, Project administration, Supervision, Validation, Writing – original draft, Writing – review & editing.

#### Declaration of competing interest

The authors declare that they have no known competing financial interests or personal relationships that could have appeared to influence the work reported in this paper.

#### Data availability

Data will be made available on request.

#### Acknowledgments

US National Science Foundation (NSF) (1827745).

#### References

- [1] A. Forbes, M. de Oliveira, M.R. Dennis, Structured light, Nat. Photonics 15 (4) (2021) 253–262.
- [2] H. Kogelnik, T. Li, Laser beams and resonators, Appl. Opt. 5 (10) (1966) 1550–1567.
- [3] A.E. Siegman, Hermite–Gaussian functions of complex argument as optical-beam eigenfunctions, J. Opt. Soc. Am. 63 (9) (1973) 1093–1094.
- [4] S. Saghafi, C.J.R. Sheppard, J.A. Piper, Characterising elegant and standard Hermite–Gaussian beam modes, Opt Commun. 191 (3) (2001) 173–179.
- [5] C. Alpmann, C. Schöler, C. Denz, Elegant Gaussian beams for enhanced optical manipulation, Appl. Phys. Lett. 106 (24) (2015).

- [6] I. Kimel, L.R. Elias, Relations between hermite and Laguerre Gaussian modes, IEEE J. Quant. Electron. 29 (9) (1993) 2562–2567.
- [7] V.V. Kotlyar, A.A. Kovalev, Hermite-Gaussian modal laser beams with orbital angular momentum, J. Opt. Soc. Am. 31 (2) (2014) 274–282.
- [8] V.V. Kotlyar, A.A. Kovalev, A.P. Porfirev, Vortex Hermite-Gaussian laser beams, Opt Lett. 40 (5) (2015) 701–704.
- [9] Y. Wang, et al., Generalised Hermite–Gaussian beams and mode transformations, J. Opt. 18 (5) (2016), 55001-55001.
- [10] M.A. Cox, et al., Structured light in turbulence, IEEE J. Sel. Top. Quant. Electron. 27 (2) (2021) 1–21.
- [11] M.A. Cox, et al., The resilience of hermite- and Laguerre-Gaussian modes in turbulence, J. Lightwave Technol. 37 (16) (2019) 3911–3917.
- [12] S. Zhao, et al., Universal understanding of self-healing and transformation of complex structured beams based on eigenmode superposition, Appl. Opt. 62 (12) (2023) 3186–3196.
- [13] M. Padgett, R. Bowman, Tweezers with a twist, Nat. Photonics 5 (6) (2011) 343-348
- [14] E. Otte, C. Denz, Optical trapping gets structure: structured light for advanced optical manipulation, Appl. Phys. Rev. 7 (4) (2020), 041308.
- [15] M.G.L. Gustafsson, Nonlinear structured-illumination microscopy: wide-field fluorescence imaging with theoretically unlimited resolution, Proc. Natl. Acad. Sci. USA 102 (37) (2005) 13081–13086.
- [16] B.-C. Chen, et al., Lattice light-sheet microscopy: imaging molecules to embryos at high spatiotemporal resolution, Science 346 (6208) (2014), 1257998-1257998.
- [17] J.-H. Jang, et al., 3D micro- and nanostructures via interference lithography, Adv. Funct. Mater. 17 (16) (2007) 3027–3041.
- [18] S.-H. Nam, et al., Photolithographic realization of target nanostructures in 3D space by inverse design of phase modulation, Sci. Adv. 8 (21) (2022) eabm6310.
- [19] A. Ortiz-Ambriz, et al., Generation of arbitrary complex quasi-non-diffracting optical patterns, Opt Express 21 (19) (2013) 22221–22231.
- [20] H.K. Meena, B.K. Singh, Controlled modulation of optical energy in the high order Hermite-Gaussian laser modes, Optik 232 (2021), 166560.
- [21] H.K. Meena, B.K. Singh, Experimental realization of modulated Hermite–Gaussian laser modes: a maximum number of highly intense lobes, J. Opt. Soc. Am. 39 (11) (2022) 2104–2109.
- [22] Y. Yuan, et al., Propagation factors of Hermite-Gaussian beams in turbulent atmosphere, Opt Laser, Technol, 42 (8) (2010) 1344–1348.
- [23] LightPipes for Python. http://www.okotech.com/lightpipes.
- [24] A. Siegman, New developments in laser resonators, in: Proc. SPIE, SPIE, 1990.
- [25] A. Siegman, Defining, measuring, and optimizing laser beam quality, Proc. SPIE 1868 (1993) 2–12. SPIE.
- [26] S. Saghafi, C.J.R. Sheppard, The beam propagation factor for higher order Gaussian beams, Opt Commun. 153 (4) (1998) 207–210.
- [27] S. Scholes, A. Forbes, Improving the beam quality factor (M2) by phase-only reshaping of structured light, Opt Lett. 45 (13) (2020) 3753–3756.